American Mineralogist, Volume 88, pages 1–10, 2003

A molecular dynamics study of the behavior of sodium in low albite

ALBERTO ALBERTI,[1,*] ETTORE FOIS,[2] AND ALDO GAMBA[2]

[1]Dipartimento di Scienze della Terra, Università di Ferrara, C.so Ercole I d'Este 32, 44100 Ferrara, Italy
[2]Dipartimento di Scienze Chimiche, Fisiche e Matematiche, Università dell'Insubria, Via Lucini 3, 22100 Como, Italy

ABSTRACT

The structural features of albite (atomic coordinates and distances, thermal displacements) at 25 and 1040 °C, obtained by Molecular Dynamic simulations following the Car-Parrinello approach, were favorably compared with those obtained by single-crystal diffraction experiments. Starting from this basis, it was shown that the marked anisotropy of electron density distribution about the positions of the sodium atoms is due to a time average of highly anisotropic thermal vibrations, and not to a space average of multiple positions occupied by Na. Although the large displacement of Na from its center of gravity results in great variations over time of the individual Na-O distances of the sodium coordination polyhedron, the average distance remains approximately constant, reaching its minimum variation when the 9 nearest O atoms are considered, thus supporting a true 9-coordination of sodium.

INTRODUCTION

Feldspars are by far the most common minerals in the Earth's crust, constituting more than 50% of it, so that their influence extends into almost all branches of geology. It is consequently of particular interest to determine their structural features and their relationships with the petrologic history of their host rocks.

The feldspar minerals are characterized by (1) an MT_4O_8 composition where T stands for atoms (normally Si and Al) in tetrahedral coordination with oxygen, and M for a larger cation (usually K, Na, or Ca) and (2) a 4-connected 3-dimensional framework with M cations in the cavities.

Two major features dominate the interpretation of the structural details of feldspars: the (Si, Al) distribution in the tetrahedral sites, and the location and coordination of the extra-framework M sites. The latter feature is particularly interesting in the sodium end-member where, in spite of a large number of structural studies (by X-ray or neutron diffraction), it is still not clear if the Na atoms are characterized by a strongly anisotropic thermal vibration or by a static disorder over two or more distinct crystallographic positions, and whether this behavior is influenced by temperature.

The aim of the present paper is to elucidate this problem by means of molecular dynamics simulations using the Car-Parrinello approach (MD from now on). The recent progress in both experimental and computational mineralogy, and in particular the dramatic increase in available computational resources and the rapid progress of software, allows us to tackle such a problem with an approach impossible only few years ago.

THE CRYSTAL STRUCTURE OF ALBITE

Following Wells (1954, 1977) the crystal structure of feldspar may be described as a 4-connected 3D net where the tetrahedral centers (nodes) are occupied by Si or Al, and the linkages are T-O-T bridges. The basic framework consists of cross-linked "double-crankshaft" chains of SiO_4 and AlO_4 tetrahedra, alternately parallel and nearly perpendicular to the **a** axis. These chains are connected through oxygen bridges along the **b** and **c** axes.

As noted previously, this paper deals with the Na end-member, whose unit cell content can be expressed as $Na_4Al_4Si_{12}O_{32}$. The topological symmetry is monoclinic $C2/m$, whereas the real symmetry is either monoclinic $C2/m$ or triclinic $C\bar{1}$. In monoclinic feldspars there are only two symmetrically nonequivalent tetrahedral sites, T1 and T2, thus complete ordering is prohibited. When the symmetry is reduced to triclinic, T1 and T2 split into T1o and T1m and into T2o and T2m respectively, enabling complete ordering (with Al in T1o). In sodium feldspar both displacive and diffusive transformations occur, which can result in changes of symmetry. Sodium feldspar shows two triclinic $C\bar{1}$ structural modifications, which differ in the degree of (Si, Al) order: (1) high albite, which has a disordered (Si, Al) distribution over the 4 tetrahedral sites; (2) low albite, the most common in nature, which presents an ordered (Si, Al) distribution with Al atoms in the T1o site and Si atoms in the other three tetrahedral sites (T1m, T2o, and T2m). Na atoms, which compensate the negative charge of the Al ↔ Si substitution, occupy the interstices of the framework.

THE SODIUM PROBLEM

From the very first structure refinements of low and high albite, performed by Ferguson et al. (1958), the highly anisotropic electron density distribution of the Na atoms was evident in both structures. A possible interpretation made by these authors is that sodium occupies at random one or other of two positions within the feldspar cage.

Ribbe et al. (1969), re-examining the data of Ferguson et al. (1958), suggested that the observed anisotropy of the Na atom in low albite can be explained either as a time average of highly anisotropic thermal vibration, or as a space average of multiple positions occupied by the sodium atoms: in the latter case,

* E-mail: alb@dns.unife.it

0003-004X/03/0001–1$05.00

a random space average over two or more positions of low potential energy—with Na atoms occupying different sites or oscillating between them—or else a faulted domain average. This problem was discussed in detail by Megaw in an Appendix to the paper (Ribbe et al. 1969); the conclusion was that "low albite is close to the limit where the models with half-atom and anisotropic atoms are interchangeable."

According to Quareni and Taylor (1971) there is little doubt that, in low albite, the observed anisotropy of Na atoms represents true anisotropic thermal vibration. The same conclusion was reached by Winter et al. (1977) on the basis of thermal expansion and anisotropy at high temperature of sodium atoms in low albite. Harlow and Brown (1980), in their X-ray and neutron diffraction study of low albite, observed that the anisotropic model appears superior, though not with any great certainty. If a displacive split-site model is accepted, an Na-Na distance of 0.39 Å is obtained.

More recently, Armbruster et al. (1990) modeled the highly anisotropic displacement parameters of low albite at room temperature either by splitting the Na position between two sites, or by refining only one site assuming anisotropic thermal vibration. They concluded that the one-site model is preferable, as their data and those of the literature indicate this model as physically correct.

According to Prewitt et al. (1976), in high albite the splitting of sodium into four-quarter atoms clearly gives the best agreement between the structure model and X-ray intensities. Winter et al. (1979) also stated that some form of static spatial disorder must exist in high albite. The same conclusion was reached by Phillips et al. (1989) who, in their study of an intermediate albite sample, affirmed that positional disorder is present in the structure.

In conclusion, the one-site model seems to be more commonly accepted for low albite, whereas the displacive split-site model (two or four sites) is commonly accepted for high albite. If the two-site model is accepted for both high and low albite, the Na-Na distance should be larger in high than in low albite. In any case the behavior of the Na atom in albite is still not well understood, and the above discussion merely reinforces the conclusions of Smith et al. (1986) that from diffraction studies, whether X-ray or neutron, further elaboration is "unprofitable."

We are now able to tackle this problem by means of a completely different approach, i.e. through the results of Molecular Dynamics calculations for low albite at room and high temperature. Computational and experimental results are compared at each step in order to verify the reliability of the calculations.

COMPUTATIONAL DETAILS

A useful method for investigating the microscopic behavior of a chemical system is the Molecular Dynamics technique, which involves the numerical solution of a set of classical equations of motion. However, the conventional MD approach is often inadequate to treat such complex events as the breaking and forming of bonds, due to insufficiently accurate description of the interatomic interactions. Forces between atoms are in fact calculated from empirical potentials, which cannot generally be transferred to different chemical environments. The Car-Parrinello method (Car and Parrinello 1985) allows us to follow the time evolution of a system at finite temperature without losing the accuracy of first principles calculations. In this approach, an extended Lagrangean formalism generates the dynamics for the system, where the electronic wavefunction coefficients $\{\psi\}$ are treated as classical degrees of freedom. The equations of motion for $\{R\}$, the nuclear positions, and $\{\psi\}$ obtained from the Car-Parrinello Lagrangean are then numerically integrated by means of standard Molecular Dynamics techniques (Allen and Tildesley 1989). The energy of the system and the forces acting on the nuclei are calculated with the Density Functional Theory (Hohenberg and Kohn 1964; Kohn and Sham 1965; Kohn 1999).

Here we present the results from first principles simulations of two low albites at 25 and 1040 °C, respectively. In both cases, the periodically repeated simulation cell—which coincides with the crystallographic unit cell—contains 52 atoms: 12 Si, 4 Al, 32 O, and 4 extra-framework Na; the total number of valence electrons is 256 (192 O, 48 Si, 12 Al, and 4 Na). The symmetry used for MD is $P1$, so that each of the 52 atoms in the unit cell is symmetrically independent. The unit-cell parameters (see Table 1) obtained from the diffraction studies discussed later were utilized for the calculations. Electron-electron interaction was calculated by adopting a gradient-corrected density functional approximation (Parr and Yang 1989; Becke 1988; Perdew 1986), while norm-conserving pseudopotentials (Troullier and Martins 1991) were used to model the electron-ion interactions; *d* nonlocality (Kleinman and Bylander 1982) was adopted for all atoms but Na (local norm-conserving pseudopotentials). The wavefunctions were expanded in plane waves up to a cutoff of 60 Ry (the cutoff for the electron density was 240 Ry), and calculated only at the Γ point because of the large unit cell of the albite crystal. The equations of motion were integrated using a time step of 0.181 femtoseconds, while a fictitious mass of 1000 a.u. (Car and Parrinello 1985) was adopted for the wavefunction coefficients. After equilibration, we followed the time evolution of sodium feldspar for 10.2 picoseconds (56.600 time steps) at a temperature of 25°, and 4.5 ps (25.000 time steps) at 1040 °C. The CPMD computer code of Hutter et al. (1996) was used for the simulations.

The mean positions of the atoms in the unit cell were calculated as follows. At each time step, the atomic coordinates were stored in histograms, one for each coordinate (x_i), in fractional units, where $i = 1, 2, 3$. The mean coordinates were then calcu-

TABLE 1. Cell parameters of albite samples used for Molecular Dynamics simulations

Sample	*a* (Å)	*b* (Å)	*c* (Å)	α (°)	β (°)	γ (°)	*V* (Å³)
Stintino 25 °C*	8.133 (1)	12.773 (5)	7.159 (5)	94.23 (4)	116.64 (4)	87.72 (2)	662.9 (5)
Tiburon 1040 °C†	8.280 (1)	12.865 (2)	7.182 (1)	93.25 (1)	116.13 (1)	87.55 (1)	685.6(2)

Note: Standard deviations in parentheses.
* Meneghinello et al (1999).
† Winter et al. (1977), see text.

lated from these frequency distributions by means of the fh,+t moment of the distribution (Willis and Prior 1975):

$$X_i^I = \frac{\int x_i^I D(x_i^I)dx}{\int D(x_i^I)dx} \quad (1)$$

where $D(^I_{xi})$ is the (unnormalized) frequency distribution function relative to the *i-th* (i = 1, 2, 3) coordinate of the *I-th* (I = 1,52) atom. In a similar way it is possible to calculate the pair distributions of coordinates of atom I, $D(^{I,\ I}_{xi,\ xj})$ where i and j = 1, 2, 3.

At the end of the simulations the structural parameters, atomic coordinates, and displacement factors of the four atoms independent in MD but symmetrically dependent in the crystallographic space group $C\bar{1}$ were averaged.

Experimental data

As anticipated in the previous section two different simulations were carried out: (1) with an ordered (Si, Al) distribution with all Al atoms in T1o at 25 °C; (2) with an ordered (Si, Al) distribution at 1040 °C. The crystal structure refinement of ordered Stintino albite (Meneghinello et al. 1999) provided the starting coordinates of atoms and the unit-cell parameters (see Table 1) for simulation (1). The structure refinement at 970 °C of ordered Tiburon albite (Winter et al. 1977) provided the starting coordinates of atoms for simulation (2), whereas the 1040 °C unit-cell parameters were obtained by extrapolation of the unit-cell data, as a function of temperature, by the same authors in their Figure 1 (see Table 1). The same structure refinements provided the anisotropic temperature factors and the interatomic distances to be compared with the results of the simulations. The ordered structure of albite from Stintino at 25 °C also provided the observed structure factors to be compared with those calculated by Molecular Dynamics (and extensively discussed in the next section).

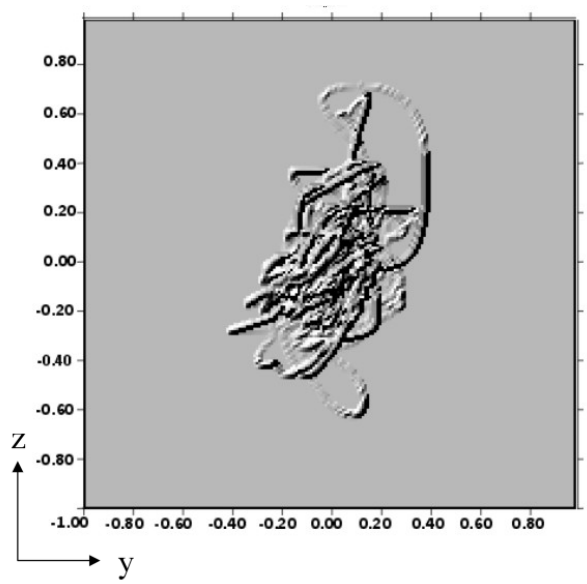

Figure 1. Evolution over time of atom Na1, in the *yz* projection.

Comparison between experimental and computational data

Structure factors

Diffraction patterns (X-ray or neutron) represent the most viable experimental approach for defining the structures of condensed matter materials. Essentially, most of what we know about crystal structure comes from diffraction experiments; in particular, atomic positions in a crystal are generally the main target of a diffraction study. On the other hand, atomic positions are the basic variable of a computer simulation study, and it is clear that the reliability of a calculated structure depends on its agreement with the direct experimental observable, i.e., the diffraction intensities. These intensities are proportional to the squared values of the structure factors F^{obs}_{hkl}, which can be calculated with the following expression:

$$F^{cal}_{hkl} = \sum_{I=1}^{m} T^I_{hkl} f^I(\theta) e^{\left[2\pi i\left(hX_1^I + kX_2^I + lX_3^I\right)\right]} \quad (2)$$

For X-ray diffraction, excluding multiple scattering, this formula is equivalent to the thermal average of the Fourier transform of total electronic density $\rho(x_1, x_2, x_3)$:

$$F^{cal}_{hkl} = \left\langle \int_V \rho(x_1, x_2, x_3) e^{\left[2\pi i(hx_1 + kx_2 + lx_3)\right]} dx_1 dx_2 dx_3 \right\rangle \quad (3)$$

The sum in Equation 2 is over the M atoms in the unitary cell; h, k, l are the indexes of the Miller planes (to which the scattering angles θ correspond), and $f^I(\theta)$ represents the scattering coefficient of the *I-th* atom in the unit cell (of volume V). X_1^I, X_2^I, X_3^I represent the mean positions, expressed in crystallographic coordinates, of the *I-th* atom, while T^I_{hkl} represents the temperature factor, which accounts for the thermal motion of the atom and modulates the diffraction of a perfect crystal by a quantity:

$$T^I_{hkl} = e^{-2p^2\left(U_{11}h^2a^{*2} + U_{22}k^2b^{*2} + U_{11}l^2c^{*2} + 2U_{12}hka^*b^* + 2U_{23}klb^*c^* + 2U_{13}hla^*c^*\right)} \quad (4)$$

where the U_{ij} values represent the atomic displacement parameters (adps) and a^*, b^*, and c^* are the reciprocal lattice parameters.

In this paper the first-principles X-ray diffraction patterns are calculated in two different ways. In the first approach, $\langle X_1^I, X^I{}_2, X^I{}_3 \rangle$ are obtained by the first moments distribution of the atomic positions. The scattering coefficients, $f^I(\theta)$, are the Fourier Transform of the isolated atomic (neutral) densities calculated by the same density functional approximation used in the simulations of the crystals. The U_{ij} for each atom I, needed for T^I_{hkl}, are calculated from the average pair distribution of the atomic positions D (x_i, y_i) using the formula:

$$U_{ij} = \frac{\iint (x_i - X_i)(x_j - X_j) D(x_i, x_j) dx_i dx_j}{\iint D(x_i, x_j) dx_i dx_j} \quad (5)$$

where i and j = 1, 2, 3. In this way Equation 2 may be used for the calculations of F^{cal}_{hkl}. In the second approach, F^{cal}_{hkl} is calculated using Equation 3. In the Car-Parrinello method it is possible to have the ground state electronic density for each atomic configuration along the trajectory. In the pseudopotential approximation adopted here, the total electronic density $\rho(r)$ is

split between valence density $\rho_{val}(r)$ and core density $\rho_{core}(r)$:

$$\rho(r) = \rho_{val}(r) + \sum_{I=1}^{M} \rho^{I}_{core}(R^{I} - r) = \rho_{val}(r) + \rho_{core}(r) \quad (6)$$

where r is a generic position in the simulation cell and R^{I} is the position of the *I-th* atom.

The total structure factor for each configuration in the simulation is therefore the sum of the Fourier Transforms of $\rho_{val}(r)$ and $\rho_{core}(r)$. $\rho^{I}_{core}(r)$ is the core density of the Na, O, Al, and Si atoms, and is calculated by the same density functional approximation used for the simulations. The total structure factors are then averaged over the trajectories in order to obtain the overall average. At each time step t, we therefore calculate:

$$F_{hkl}(t) = F^{val}_{hkl}(t) + F^{core}_{hkl}(t) \quad (7)$$

$$F^{val}_{hkl}(t) = \left\langle \int_{V} p\mathrm{val}(x_1, x_2, x_3) e^{[2\pi i(hx_1 + kx_2 + lx_3)]} \mathrm{d}v \right\rangle \quad (8)$$

$$F^{core}_{hkl}(t) = \sum_{I=1}^{M} \rho^{I}_{core}(h,k,l) e^{\left[2\pi i\left(hx^{I}_1 + kx^{I}_2 + lx^{I}_3\right)\right]} \quad (9)$$

where the vectors $\{x^{I}_1, x^{I}_2, x^{I}_3\}$ are the positions, in crystallographic (fractional) units, of the *I-th* atom for the configuration at time t along the trajectory.

In a typical structure refinement by diffraction data, its accuracy can be roughly evaluated by the value of the discrepancy factor

$$R = \frac{\sum_{hkl} || F^{obs}_{hkl} | - | F^{cal}_{hkl} ||}{\sum_{hkl} | F^{obs}_{hkl} |} \quad (10)$$

which, in an acceptable refinement, is below 0.1. Computer simulations allow the calculation of $\langle X^{I}_1, X^{I}_2, X^{I}_3 \rangle$ and of T^{I}_{hkl}, hence the direct evaluation of $(F^{cal}_{hkl}\}$, and Equation 10 may be used to compare the calculated structure versus the experimental results.

This comparison was made using the observed structure factors measured for the ordered Stintino albite at 25 °C with $F_{obs} > 6\sigma(F_{obs})$ in the range $0 < \theta < 48°$ (3980 reflections), and gave $R = 0.06$ for the F^{cal}_{hkl} calculated from first principles (Eq. 7) and $R = 0.044$ for the F^{cal}_{hkl} calculated from the structure refinement (Meneghinello et al. 1999).

Atomic coordinates

Table 2 reports the atomic coordinates obtained by MD at 25 and 1040 °C, respectively. There is an acceptable agreement between these coordinates and those given by Meneghinello et al. (1999) for Stintino albite at 25 °C and by Winter et al. (1977) for Tiburon albite at 970 °C. However, remarkable differences (up to 40 times the standard deviation of the experimental values) occur in some cases. If we now calculate the structure factors of albite at 25 °C using the atomic coordinates and the atomic displacement parameters (reported in Table 4) obtained by MD (Eq. 2), and compare them with the observed structure factors for Stintino albite at 25 °C, the discrepancy factor R is as high as 0.236 [for $F_{obs} > 6\sigma(F_{obs})$], indicating an apparently inadequate agreement between the MD results and experimental atomic coordinates. However, if the structure factors are calculated after each step of MD according to Equation 7 and averaged at the end of the simulation, the discrepancy factor is only 0.06, as reported in the previous paragraph. This result is extremely important as it implies that MD simulates very well the relative motion of the atoms, i.e., the relative phases of the atoms at each time step contribute correctly to the observed diffracted intensity.

TABLE 2. Atomic coordinates obtained by Molecular Dynamics simulations

	25 °C			1040 °C		
	x	*y*	*z*	*x*	*y*	*z*
Na	0.2680	0.9929	0.1438	0.2775	0.9898	0.1486
T1o	0.0072	0.1661	0.2054	0.0079	0.1728	0.2097
T1m	0.0005	0.8213	0.2409	0.0034	0.8222	0.2407
T2o	0.6887	0.1081	0.3081	0.6939	0.1131	0.3196
T2m	0.6735	0.8810	0.3625	0.6853	0.8840	0.3614
OA1	0.0076	0.1263	0.9610	0.0055	0.1328	0.9668
OA2	0.5805	0.9967	0.2758	0.5958	1.0003	0.2793
OBo	0.8048	0.1024	0.1758	0.8058	0.1195	0.1888
OBm	0.8119	0.8473	0.2587	0.8208	0.8540	0.2577
OCo	0.0026	0.3013	0.2753	0.0176	0.3077	0.2722
OCm	0.0212	0.6937	0.2257	0.0255	0.6961	0.2469
ODo	0.2144	0.1059	0.3853	0.2054	0.1083	0.3909
ODm	0.1793	0.8701	0.4429	0.1784	0.8720	0.4332

It is interesting to correlate the variations of atomic coordinates between 1040 and 25 °C found by MD (ΔMD) with those between 970 °C (Winter et al. 1977) and 25 °C (Meneghinello et al. 1999) determined by X-ray experiments (ΔEX). The expected correlation equation is:

$$\Delta\mathrm{MD} = (1 + \delta)\,\Delta\mathrm{EX} + b \quad (11)$$

where b is about zero and δ is a small positive value, which takes into account that MD is averaged at 1040 °C, whereas the experimental data were collected at 970 °C (Winter et al. 1977). The resulting correlation equation is:

$$\Delta\mathrm{MD} = 1.097\ (0.061)\ \Delta\mathrm{EX} + 0.000 \quad (F = 327) \quad (12)$$

Interatomic distances

Table 3 reports the T-O distances determined by MD and by X-ray diffraction, and the differences between them. If the T-O distances are compared we observe that the differences, within the same tetrahedron, determined by MD faithfully follow those found experimentally, at both low and high temperature.

We note that the Si-O and Al-O distances determined by MD differ from those found by X-ray diffraction by about 0.010–0.015 Å and 0.030–0.040 Å, respectively. It is hard to explain whether this has a physical significance (i.e., if the divergences in the Δ values for Si and Al tetrahedra can be related to the valence of Si and Al, and, consequently, to the Si-O and Al-O bond strengths) or whether the approximations inherent in the model used for the simulations also affect these results.

Anisotropic displacement factors

As indicated previously, the U_{ij} parameters for each atom are calculated from the average pair distribution of the atomic positions, using Equation 5. Table 4 reports, for each atom, the length of the principal axes of the anisotropic thermal ellipsoids and the equivalent temperature factors, at 25 °C by MD

TABLE 3. T-O distances from experimental data and Molecular Dynamics simulations

	Men 25 °C	MD 25 °C	Δ	Win 970 °C	MD 1040 °C	Δ
T1o-OA1	1.748	1.787	0.039	1.742	1.782	0.040
T1o-OBo	1.742	1.785	0.043	1.740	1.777	0.037
T1o-OCo	1.729	1.766	0.037	1.735	1.764	0.029
T1o-ODo	1.740	1.785	0.045	1.741	1.785	0.044
T1m-OA1	1.598	1.611	0.013	1.593	1.600	0.007
T1m-OBm	1.601	1.615	0.014	1.594	1.604	0.010
T1m-OCm	1.621	1.632	0.011	1.616	1.625	0.009
T1m-ODm	1.614	1.627	0.013	1.616	1.624	0.008
T2o-OA2	1.635	1.650	0.015	1.625	1.643	0.018
T2o-OBo	1.593	1.606	0.013	1.581	1.591	0.010
T2o-OCm	1.614	1.629	0.015	1.622	1.629	0.007
T2o-ODm	1.614	1.625	0.011	1.611	1.622	0.011
T2m-OA2	1.645	1.663	0.018	1.647	1.660	0.013
T2m-OBm	1.617	1.634	0.017	1.616	1.621	0.005
T2m-OCo	1.597	1.612	0.015	1.594	1.601	0.007
T2m-ODo	1.601	1.616	0.015	1.595	1.601	0.006

Notes: Men = Meneghinello et al. (1999); Win = Winter et al. (1977); MD = Molecular Dynamics, this work.

and by X-ray crystal structure refinements from the literature. Table 5 reports the orientation of the principal axes with respect to an orthogonal Cartesian system. Tables 6 and 7 report the same data for MD at 1040 °C and for Tiburon albite at 970 °C.

With respect to the length of the principal axes, there is a satisfactory agreement between the MD and X-ray data, even if MD tends to emphasize the anisotropy of the atoms, in particular of the O atoms in the rings of four tetrahedra of the "double crankshaft," i.e., the OB, OC, and OD O atoms, which also show slightly larger B_{eq} values with respect to those of the X-ray refinements. With respect to the orientation of the principal axes of the ellipsoids we can see that, for the above-mentioned oxygen atoms, there is an excellent agreement between MD and X-ray data, less satisfactory for the other atoms. We observe, however, that analogous discrepancies also exist between the data of different X-ray refinements (see Tables 5 and 7). An explanation of these results may be found in the lower anisotropy of the other atoms, where slight variations in the U_{ij} values can cause remarkable variations in the orientation of the ellipsoids; this is particularly true for the two smaller, more similar axes. In fact, we verified that variations in the U_{ij} of X-ray data equal to their standard deviation can modify the angles of the principal axes of the ellipsoids with respect to our orthogonal Cartesian system by up to 20°. We note that, in order to have the same orientation of the ellipsoids from MD and X-ray data, the R1 and R2 axes of atoms T1m and T2m at 25 °C, and of atoms T2o and T2m at 1040 °C, must be interchanged. In conclusion, there is a satisfactory agreement between the thermal parameters given by MD and those obtained experimentally.

ANALYSIS OF NA BEHAVIOR

Starting from the above results it is now possible to study the behavior of Na atoms in albite, focusing our attention on the following two points. (1) Is the highly anisotropic electron density distribution of Na due to a time or space average? (2) Can the irregular coordination of Na (5, 5 + 2, 7 + 2) be better understood with the help of MD, when point 1 is clarified?

TABLE 4. Albite 25 °C. Apparent thermal parameters: root-mean square amplitude (Å)

Site		Men	Arm	W&K	H&B	MD
Na	R1	0.123	0.113	0.113	0.116	0.093
	R2	0.124	0.128	0.130	0.130	0.134
	R3	0.261	0.262	0.240	0.256	0.297
	Beq	2.63	2.57	2.29	2.53	3.02
T1o	R1	0.068	0.076	0.071	0.072	0.061
	R2	0.086	0.079	0.074	0.075	0.076
	R3	0.101	0.090	0.086	0.096	0.106
	Beq	0.61	0.53	0.47	0.53	0.54
T1m	R1	0.071	0.072	0.061	0.066	0.061*
	R2	0.083	0.074	0.070	0.068	0.055*
	R3	0.096	0.088	0.083	0.090	0.101
	Beq	0.55	0.49	0.41	0.44	0.45
T2o	R1	0.071	0.074	0.070	0.064	0.047
	R2	0.090	0.078	0.075	0.078	0.061
	R3	0.096	0.089	0.086	0.090	0.100
	Beq	0.59	0.51	0.47	0.46	0.42
T2m	R1	0.074	0.071	0.067	0.063	0.058*
	R2	0.080	0.080	0.074	0.081	0.050*
	R3	0.097	0.087	0.082	0.084	0.096
	Beq	0.56	0.51	0.44	0.46	0.40
OA1	R1	0.070	0.075	0.081	0.072	0.074
	R2	0.110	0.111	0.107	0.098	0.104
	R3	0.140	0.128	0.129	0.141	0.121
	Beq	0.97	0.90	0.91	0.92	0.82
OA2	R1	0.074	0.072	0.075	0.075	0.050
	R2	0.090	0.086	0.082	0.094	0.059
	R3	0.111	0.115	0.114	0.119	0.137
	Beq	0.69	0.68	0.67	0.75	0.65
OBo	R1	0.072	0.080	0.080	0.092	0.063
	R2	0.116	0.110	0.107	0.110	0.111
	R3	0.145	0.138	0.138	0.137	0.154
	Beq	1.05	0.99	0.97	1.03	1.06
OBm	R1	0.079	0.075	0.072	0.085	0.064
	R2	0.123	0.137	0.139	0.132	0.153
	R3	0.168	0.152	0.151	0.151	0.165
	Beq	1.30	1.25	1.25	1.26	1.43
OCo	R1	0.082	0.081	0.081	0.079	0.055
	R2	0.106	0.105	0.102	0.116	0.091
	R3	0.128	0.126	0.123	0.126	0.199
	Beq	0.92	0.88	0.84	0.95	1.34
OCm	R1	0.081	0.077	0.076	0.076	0.055
	R2	0.114	0.105	0.103	0.108	0.089
	R3	0.124	0.131	0.128	0.140	0.207
	Beq	0.94	0.90	0.86	0.98	1.41
ODo	R1	0.090	0.082	0.082	0.082	0.061
	R2	0.114	0.111	0.111	0.110	0.107
	R3	0.122	0.133	0.133	0.145	0.178
	Beq	0.97	0.96	0.97	1.05	1.24
ODm	R1	0.090	0.081	0.081	0.084	0.053
	R2	0.118	0.120	0.121	0.115	0.135
	R3	0.145	0.146	0.144	0.157	0.232
	Beq	1.16	1.11	1.11	1.19	1.97

Notes: Men = Meneghinello et al. (1999); Arm = Armbruster et al. (1990); W&K = Wenk and Kroll (1984) ionic model in Table 8; H&B = Harlow and Brown (1980); MD = Molecular Dynamics, this work.

Analysis of thermal ellipsoids

As indicated in the previous section, this point has not been answered to the satisfaction of all researchers; the one-site model is preferred for low albite, whereas the displacive split-site model is commonly accepted for high albite. In the present

TABLE 5. Angles (°) of principal axes R1, R2, R3 (Table 3) with respect to an orthogonal Cartesian system *x, y, z* oriented as follows: *x* axis along *a*, *y* axis along $(a \times b) \times a$, *z* axis along c^*

		R1			R2			R3		
		x	*y*	*z*	*x*	*y*	*z*	*x*	*y*	*z*
Na	Men	19	88	72	106	55	40	81	35	125
	Arm	36	79	56	124	56	52	79	36	124
	W&K	57	65	44	146	66	67	83	36	125
	H&B	86	55	35	166	77	86	77	38	125
	MD	56	84	35	127	42	72	55	49	119
T1o	Men	135	119	59	92	135	135	45	121	62
	Arm	122	120	47	109	129	135	38	127	81
	W&K	129	100	41	124	125	127	58	143	74
	H&B	96	110	21	108	154	108	19	105	79
	MD	118	131	55	102	137	130	32	101	60
T1m	Men	45	86	134	75	163	81	131	106	134
	Arm	64	87	154	56	140	72	135	130	108
	W&K	61	80	149	58	136	64	134	132	105
	H&B	75	75	158	77	156	71	160	107	100
	MD	79	53	150	66	147	70	152	107	111
T2o	Men	62	28	93	33	118	106	75	95	16
	Arm	77	15	82	37	105	123	56	91	34
	W&K	85	12	79	33	92	123	58	101	35
	H&B	89	9	81	62	97	151	28	95	62
	MD	67	49	51	66	138	121	35	96	55
T2m	Men	116	149	75	150	61	83	104	100	163
	Arm	117	148	75	146	59	77	109	97	160
	W&K	127	141	79	131	52	65	116	98	153
	H&B	100	170	89	107	86	18	160	99	108
	MD	102	155	69	123	65	47	143	93	127
OA1	Men	62	81	150	87	171	99	152	88	118
	Arm	67	80	155	89	170	100	157	86	113
	W&K	71	84	160	86	171	98	160	84	109
	H&B	71	89	161	83	172	93	159	82	109
	MD	85	81	169	47	137	94	136	49	100
OA2	Men	72	19	95	24	106	73	105	80	18
	Arm	88	12	101	25	97	66	115	81	27
	W&K	90	5	95	28	92	62	118	86	28
	H&B	83	8	92	40	95	50	129	84	40
	MD	77	19	103	56	109	42	142	87	52
OBo	Men	157	109	77	99	148	121	69	115	34
	Arm	156	113	84	104	138	129	72	123	39
	W&K	154	116	86	108	135	129	71	123	40
	H&B	149	120	82	109	138	126	67	117	37
	MD	143	117	67	126	136	112	82	122	33
OBm	Men	158	71	80	105	156	71	106	104	158
	Arm	157	70	79	103	149	63	109	112	150
	W&K	157	69	80	104	150	64	107	111	152
	H&B	142	54	80	121	142	70	110	101	157
	MD	148	61	78	118	134	64	104	118	147
OCo	Men	120	148	100	149	63	77	83	75	164
	Arm	114	151	106	151	63	80	74	80	161
	W&K	112	152	107	157	67	89	83	75	163
	H&B	93	164	106	124	75	38	34	83	123
	MD	115	138	121	120	48	57	41	87	131
OCm	Men	103	19	103	16	75	84	99	79	15
	Arm	114	27	101	49	64	52	129	83	40
	W&K	112	23	97	44	68	54	126	82	37
	H&B	106	17	94	61	78	32	146	78	59
	MD	109	21	100	55	70	42	139	82	50
ODo	Men	82	75	163	82	162	106	169	100	84
	Arm	82	73	154	70	148	114	151	116	79
	W&K	74	81	161	67	153	105	152	116	79
	H&B	73	63	147	81	147	121	161	107	80
	MD	75	78	160	77	159	105	159	107	79
ODm	Men	111	110	150	98	155	66	157	75	74
	Arm	110	102	156	96	164	75	159	80	72
	W&K	107	104	158	93	166	77	163	89	73
	H&B	106	109	155	95	161	71	164	89	74
	MD	105	110	154	92	159	69	165	83	77

Notes: Men = Meneghinello et al. (1999); Arm = Armbruster et al. (1990); W&K = Wenk and Kroll (1984) ionic model in Table 8; H&B = Harlow and Brown (1980); Molecular Dynamics, this work.

TABLE 6. Albite 1040 °C. Apparent thermal parameters: root-mean square amplitude (Å)

	Win				MD			
	R1	R2	R3	B_{eq}	R1	R2	R3	B_{eq}
Na	0.256	0.306	0.472	10.05	0.198	0.314	0.488	9.88
T1o	0.151	0.156	0.185	2.14	0.108	0.146	0.236	2.33
T1m	0.144	0.149	0.178	1.97	0.103	0.122	0.219	1.94
T2o	0.141	0.160	0.178	2.03	0.127*	0.088*	0.227	1.98
T2m	0.142	0.161	0.175	2.02	0.126*	0.094*	0.202	1.73
OA1	0.148	0.226	0.261	3.72	0.146	0.218	0.242	3.35
OA2	0.143	0.179	0.240	2.89	0.110	0.121	0.314	3.30
OBo	0.161	0.236	0.268	4.05	0.136	0.259	0.290	4.47
OBm	0.159	0.268	0.284	4.67	0.132	0.279	0.368	6.08
OCo	0.160	0.215	0.255	3.60	0.119	0.197	0.372	5.03
OCm	0.149	0.220	0.257	3.60	0.125	0.189	0.386	5.28
ODo	0.165	0.225	0.260	3.82	0.106	0.247	0.335	4.84
ODm	0.161	0.237	0.279	4.22	0.098	0.257	0.392	6.05

Notes: Win = Winter et al. (1977) 970 °C; MD = Molecular Dynamics, this work.
* For explanation see text, page 5.

TABLE 7. Albite 1040 °C. Angles (°) of principal axes *R*1, *R*2, *R*3 (Table 6) with respect to an orthogonal Cartesian system *x, y, z* oriented as follows: *x* axis along *a*, *y* axis along $(a \times b) \times a$, *z* axis along c^*

		R1			R2			R3		
		x	y	z	x	y	z	x	y	z
Na	Win	26	88	64	112	53	45	76	38	124
	MD	57	85	34	124	39	73	52	51	118
T1o	Win	61	59	135	72	48	47	34	123	81
	MD	61	76	147	83	21	70	30	105	64
T1m	Win	109	86	20	120	34	104	37	57	76
	MD	122	72	38	100	30	118	34	67	66
T2o	Win	72	21	81	49	110	47	134	84	44
	MD	79	19	74	61	109	36	148	89	58
T2m	Win	101	15	101	34	75	61	121	86	32
	MD	101	20	107	58	70	40	145	89	55
OA1	Win	110	98	22	91	8	82	21	92	70
	MD	103	101	17	98	12	81	16	96	75
OA2	Win	93	174	86	144	90	126	54	96	144
	MD	97	172	85	123	82	146	33	93	123
OBo	Win	156	112	81	86	122	148	67	140	59
	MD	143	109	59	71	119	144	59	144	73
OBm	Win	155	68	79	101	141	53	112	121	141
	MD	149	64	75	94	128	38	121	131	124
OCo	Win	114	151	105	143	61	112	64	87	153
	MD	116	135	114	115	45	124	37	90	127
OCm	Win	113	26	102	38	64	64	119	90	29
	MD	110	28	109	60	62	43	142	85	52
ODo	Win	107	73	155	75	153	112	157	110	79
	MD	105	74	158	76	162	102	159	99	72
ODm	Win	109	102	157	103	159	73	157	73	75
	MD	107	107	156	97	163	75	162	88	72

Notes: Win = Winter et al. (1977); MD = Molecular Dynamics, this work.

work we used the following strategy: subsequent to the simulations the principal axes of the thermal ellipsoids of the four Na atoms, obtained using the atomic displacement parameters U_{ij} calculated from Equation 5, were rotated so that *R*1, *R*2, and *R*3 coincided with the axes *x*, *y*, and *z* of an orthogonal Cartesian system. The coordinates of the Na atoms for all steps of the simulations were referred to this orthogonal system. Figure 1 shows the evolution over time in the *yz* projection of atom Na1. It is evident that the above data set does not solve our problem, at least as it appears in Figure 1. In this case, in fact, the information is characterized by short-wavelength (in the commonly used sense) signals, superposed on each other; the best way to obtain a more stable or long-wavelength signal is to apply a suitable low-pass filter. Starting from the above 2D distribution the first step was to apply a 2D Fourier trans-

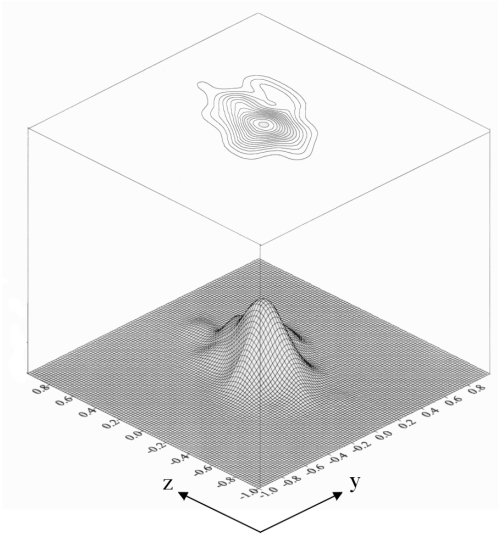

FIGURE 2. Distribution of coordinates of Na1 after the application of a low-pass filter to the Molecular Dynamics simulation shown in Figure 1.

form, then to multiply the Fourier coefficients by a precomputed set of Fourier coefficients of the chosen low-pass filter in the frequency domain, and finally to transform the product matrix back to the initial space domain. The chosen filter is of the gaussian type,

$$F = \exp\,[\,-(x - x_0)^2/\sigma] \qquad (13)$$

which is characterized by a smooth slope, and which can easily be adapted to remove the undesired frequency bands from the data, simply by varying σ. In this case a value of 0.5 for σ was chosen.

The distribution of the Na1 coordinates can be represented with a commonly used graphics program (SURFER in this case), as is shown in Figure 2. The presence of a unique Na1 peak is now evident. With the same procedure we obtained the distributions of the other Na sites (Na2, Na3, Na4). In all cases the presence of only one Na site was evident. The same procedure was then applied to the average distribution of the four Na atoms; the results are shown in Figures 3 and 4. The results indicate, beyond any doubt, that only one site is occupied by Na at 25 °C. Figures 5 and 6 show the Na distribution at 1040 °C; in this case only one Na site is evident. We conclude that at both low and high temperatures the highly anisotropic electron density distribution of Na in low albite is due to dynamic disorder, and not to a space average of multiple positions of the atoms.

Analysis of Na-polyhedron

Table 8 reports the Na-O distances found experimentally and by Molecular Dynamics simulations. We note that (1) the shortest Na-O distances (to OA2, ODo, and OBo) determined by MD are shorter than those found experimentally, and (2) the variation in Na-O distances with temperature is about the same as measured by MD and by diffraction experiments.

The environment of sodium in low albite is characterized

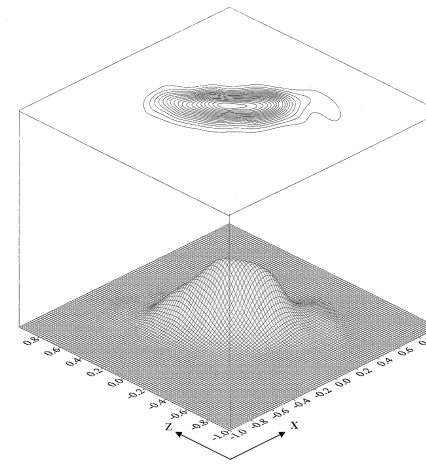

FIGURE 3. Distribution of coordinates of Na at 25 °C in the *xz* projection, after the application of a low-pass filter.

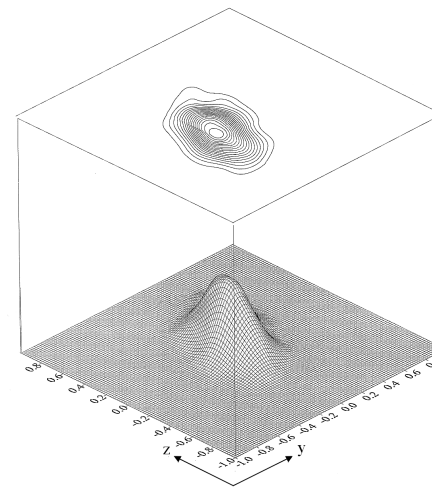

FIGURE 4. Distribution of coordinates of Na at 25 °C in the *yz* projection, after the application of a low-pass filter.

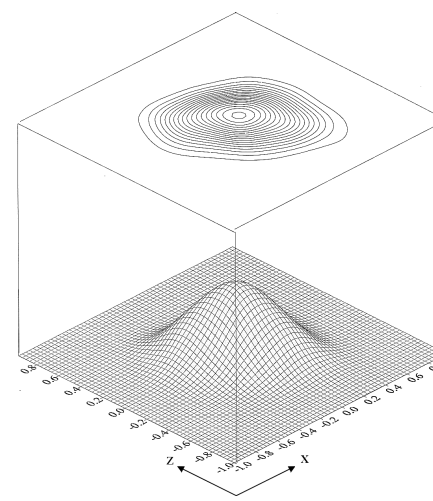

FIGURE 5. Distribution of coordinates of Na at 1040 °C in the *xz* projection, after the application of a low-pass filter.

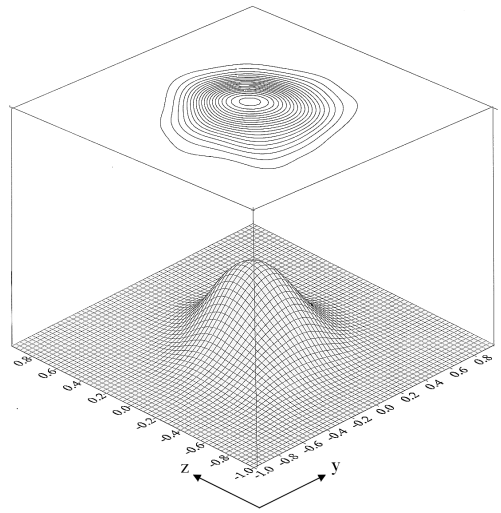

FIGURE 6. Distribution of coordinates of Na at 1040 °C in the *yz* projection, after the application of a low-pass filter.

TABLE 8. Na-O distances from experimental data and Molecular Dynamics simulations

	Men 25 °C	MD 25 °C	Δ	Win 970 °C	MD 1040 °C	Δ
Na - OA2	2.36	2.28(6)	–0.08	2.47	2.38(13)	–0.09
Na - ODo	2.44	2.35(8)	–0.09	2.59	2.50(19)	–0.09
Na - OBo	2.46	2.35(8)	–0.11	2.62	2.56(20)	–0.06
Na - OA1	2.53	2.55(8)	+0.02	2.68	2.67(21)	–0.01
Na - OA1	2.67	2.58(10)	-0.09	2.79	2.74(22)	–0.05
Na - OCo	2.97	2.98(10)	+0.01	2.92	2.92(22)	0.00
Na - ODm	3.01	3.09(10)	+0.08	2.99	3.01(22)	+0.02
Na - OCm	3.26	3.22(11)	–0.04	3.29	3.32(21)	+0.03
Na - OBm	3.47	3.47(13)	0.00	3.40	3.45(31)	+0.05
Average 5	2.49	2.42(4)	–0.07	2.63	2.57(9)	–0.06
Average 7	2.63	2.60(3)	–0.03	2.72	2.68(7)	–0.04

Notes: Men = Meneghinello et al. (1999); Win = Winter et al. (1977); MD = Molecular Dynamics, this work.

by five oxygen atoms at short distances (2.3–2.6 Å), two at about 3 Å, and two more at large distances (around 3.3–3.5 Å). The two latter distances seem too large to be considered as bond lengths for a relatively small cation like sodium. However, in microcline, where potassium has the same environment as sodium in albite, K is commonly assumed to be 9-coordinated. The nine K-O distances are in fact in the range 2.75–3.35 Å (Blasi et al. 1987). If the Na-O polyhedron in albite is compared with the K-O polyhedron in microcline, we see that five of the shorter K-O distances are strongly reduced (from 0.2 up to 0.4 Å), the two intermediate ones do not change remarkably, and the two greatest distances increase by about 0.1 Å; consequently, Na is usually assumed to be at least sevenfold-coordinated. However, the five short distances are strongly influenced by temperature, increasing by about 0.2 Å from 13 (Smith et al. 1986) to 1243 K (Winter et al. 1977); the two distances at about 3 Å decrease slightly, whereas the two largest distances do not change noticeably as the temperature increases (see Table 8); consequently, the coordination of Na is more regular at higher temperatures and the structure of albite becomes more similar to that of microcline.

Figures 7 and 8 show the Na-O radial distribution functions g(*r*), and their integrals N(*r*) at low and high temperature. It is evident from the integral function that, in spite of the definite differences between the five short, two intermediate, and two large Na-O distances, the coordination of sodium varies continuously. This shows that the individual Na-O distance varies

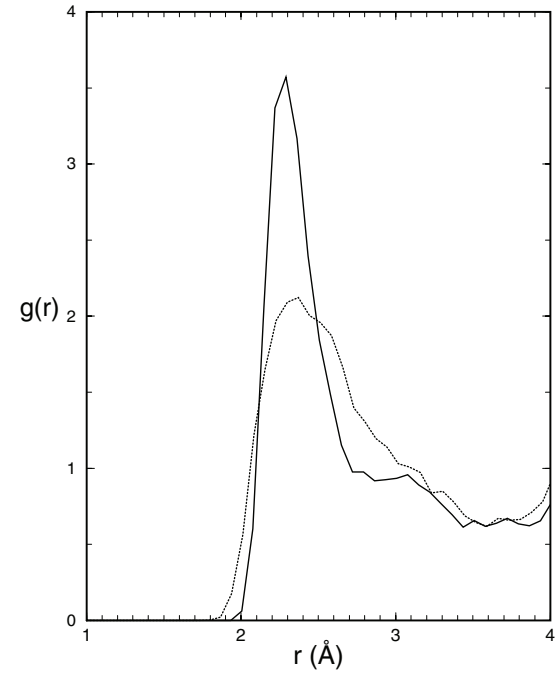

FIGURE 7. Na-O radial distribution function, g(*r*), at 25 °C (continuous line) and 1040 °C (dotted line).

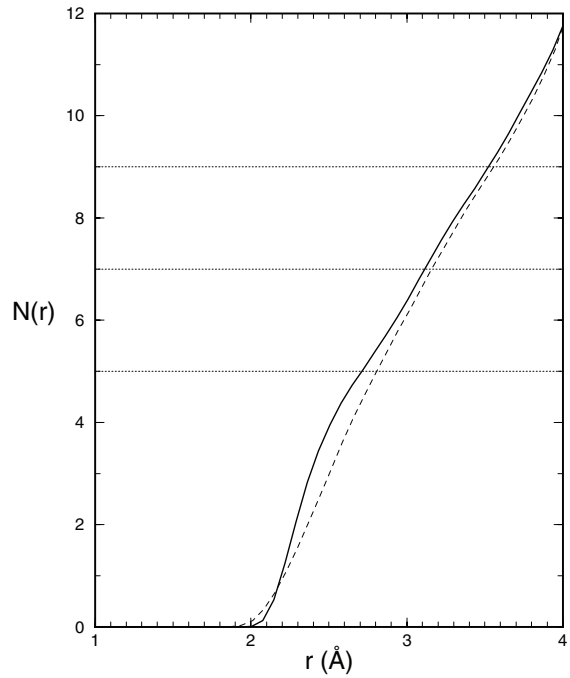

FIGURE 8. Na-O current coordination number, N(*r*), at 25 °C (continuous line) and 1040 °C (dashed line). N(*r*) values 5, 7, and 9 are indicated by dotted lines.

remarkably over time. It is therefore of interest to investigate whether the mean Na-O coordination distance also varies remarkably over time. Figure 9 shows the variations of the individual Na-O distances and of their average values for the 5 and 7 nearest oxygen atoms, at low and high temperature, over a period of 2 picoseconds (about 10 000 MD steps). It is evident that, while the individual Na-O distances can vary by more than 0.5 Å at low temperature, and by 1 Å at high temperature, the average distance remains constant within a range of 0.1 and 0.2 Å at low and high temperature, respectively. This result is confirmed by the data in Table 8. In fact, while the standard deviation of the individual Na-O distances is around 0.08 and 0.20 Å at low and high temperatures respectively, the standard deviation of the average T-O distance is far lower. It is interesting to note that, in spite of the higher values of σ for the two greater Na-O distances, the standard deviation of the average Na-O distance is lower for the 7 coordination than for the 5 coordination case, at both low and high temperature. These effects are still more evident if we consider the two longest Na-O distances. Molecular Dynamics simulations show that these two distances vary strongly over time (from 2.5 Å up to 4.5 Å): this alone gives no information about the interaction of sodium with these atoms. However, if we now consider Figure 10—where the average Na-O distance, over a period of 2 picoseconds, is reported for the 5, 7, and 9 oxygen coordinations respectively—it is evident that this distance varies, at both low and high temperature, by a lesser amount when all 9 O atoms are considered. Moreover, the standard deviation of the average distance further decreases (see Table 8). This result also demonstrates the strong interaction of the sodium atoms with the two farthest O atoms, which tend to stabilize the volume of the cation's coordination polyhedron, thus supporting a true ninefold-coordination of Na.

Also of interest is the behavior of Na atoms with respect to their nearest Na neighbors. At low temperature a sodium atom is quite close to three other Na atoms: one of these, related by the inversion centre, is situated at a distance of approximately 3.9 Å, the other two at about 4.8 and 5.1 Å respectively. This Na organization is clearly shown by the Na-Na g(r) function reported in Figure 11. The same functions for albite at high

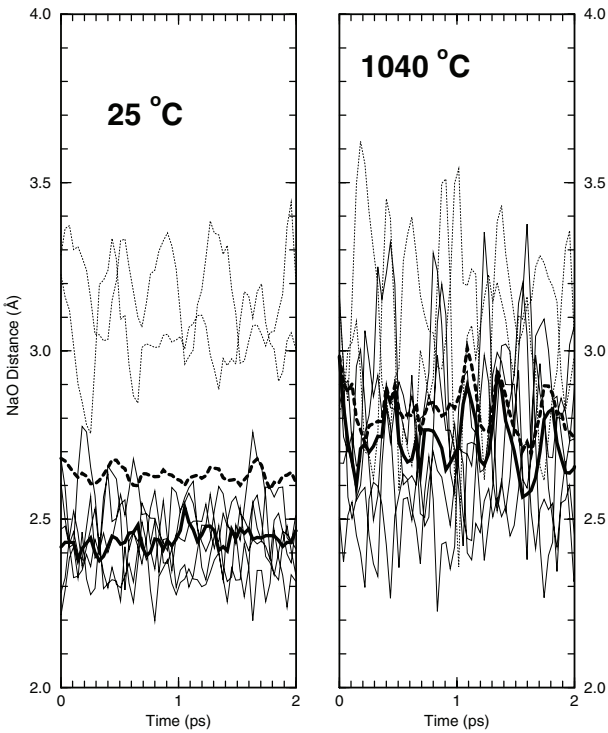

FIGURE 9. Variation over a period of 2 picoseconds of the 7 individual shorter Na-O distances (thin continuous lines for the 5 shortest distances, thin dotted lines for the other two), and of the average Na-O distances 5 and 7 (heavy continuous and dashed lines, respectively).

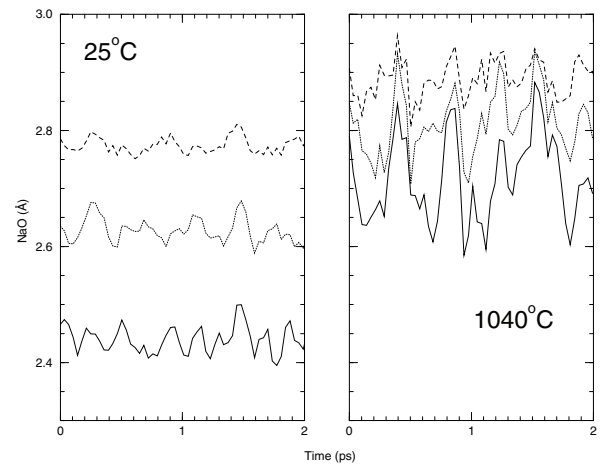

FIGURE 10. Variation over a period of 2 picoseconds of the average of the 5, 7, and 9 Na-O distances (continuous, dotted, and dashed lines, respectively).

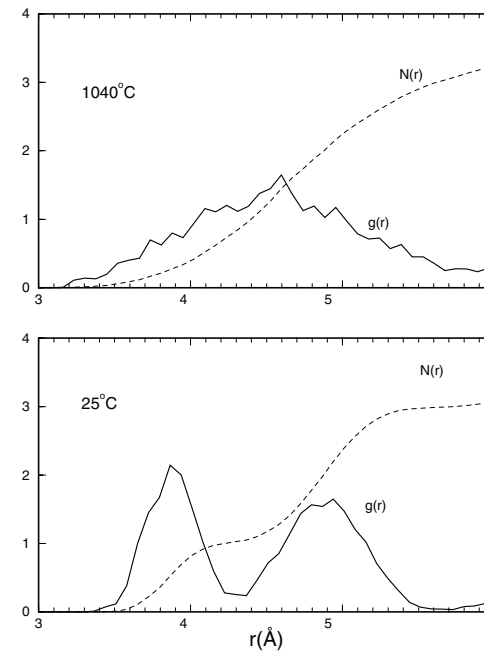

FIGURE 11. Na-Na radial distribution function g(r) (continuous line) and current coordination number N(r) (dashed line) at 25 °C, lower panel, and 1040 °C, upper panel.

temperature are also reported: in this case the apparent Na-Na distances are distributed over a large "bell-shaped" curve, reaching its maximum at about 4.6 Å. The distances between the centers of gravity of atoms do not change dramatically with temperature; in fact, at high temperature the Na-Na distances are about 4.1, 4.8, and 5.0 Å, respectively, not remarkably different from those at low temperature. It is therefore evident that the Na-Na g(r) function at high temperature is strongly influenced by the thermal motion, which causes dramatic variations of the Na-Na distances over time.

ACKNOWLEDGMENTS

We thank G. Santarato and N. Abu Zaid for their help in the use of the MATLAB program and G. Cruciani for useful comments and discussion. Italian MURST ("Transformations, reactions, ordering in minerals" COFIN 1999) is acknowledged for financial support.

REFERENCES CITED

Allen, M.P. and Tildesley, D.J. (1989) Computer Simulation of Liquids. 385 p. Clarendon Press, Oxford, U.K.

Armbruster, T., Bürgi, H.B., Kunz, M., Gnos, E., Brönnimann, S., and Lienert, C. (1990) Variation of displacement parameters in structure refinements of low albite. American Mineralogist, 75, 135–140.

Becke, A.D. (1988) Density-functional exchange-energy approximation with correct asymptotic behaviour. Physical Review, A38, 3098–3100.

Blasi, A., De Pol Blasi, C., and Zanazzi, P.F. (1987) A re-examination of the Pellotsalo microcline: mineralogical implications and genetic considerations. Canadian Mineralogist, 25, 527–537.

Car, R. and Parrinello, M. (1985) Unified approach for Molecular Dynamics and Density Functional Theory. Physical Review Letters, 55, 2471–2474.

Ferguson, R.B., Traill, R.J., and Taylor, W.H. (1958) The crystal structure of low-temperature and high-temperature albite. Acta Crystallographica, 11, 331–348.

Harlow, G.E. and Brown, G.E. (1980) Low albite: an X-ray and neutron diffraction study. American Mineralogist, 65, 986–995.

Hohenberg, P. and Kohn, W. (1964) Inhomogeneous electron gas. Physical Review B, 136, 864–868.

Hutter, J., Ballone, P., Bernasconi, M., Focher, P., Fois, E., Goedecker, S., Parrinello, M., and Tuckerman, M. CPMD code Version 3.0 MPI for Solid State Physics (Stuttgart) and IBM Research (Zurich) (1990–1996).

Kleinman, L. and Bylander, D.M. (1982) Efficacious form for model pseudopotentials. Physical Review Letters, 48, 1425–1428.

Kohn, W. (1999) Nobel Lecture: Electronic structure of matter-wave functions and density functionals. Review of Modern Physics, 71, 1253–1266.

Kohn, W. and Sham, L.J. (1965) Self-consistent equations including exchange and correlation effects. Physical Review, A140, 1135–1141.

Meneghinello, E., Alberti, A., and Cruciani, G. (1999) Order-disorder process in the tetrahedral sites of albite. American Mineralogist, 84, 1144–1151.

Parr, R.G. and Yang, W. (1989) Density functional theory of atoms and molecules. 333 p. Oxford University Press, Oxford, U.K.

Perdew, J.P. (1986) Density-functional approximation to the correlation energy of the inhomogeneous electron gas. Physical Review, B33, 8822–8824.

Phillips, M.W., Ribbe, P.H., and Pinkerton, A.A. (1989) Structure of intermediate albite, $NaAlSi_3O_8$. Acta Crystallographica, C45, 542–545.

Prewitt, C.T., Sueno, S., and Papike, J.J. (1976) The crystal structures of high albite and monalbite at high temperature. American Mineralogist, 61, 1213–1225.

Quareni, S. and Taylor W.H. (1971) Anisotropy of sodium atom in low albite. Acta Crystallographica, B27, 281–285.

Ribbe, P.H., Megaw, H.D., Taylor, W.H., Ferguson, R.B., and Traill, R.J. (1969) The albite structures. Acta Crystallographica, B27, 1503–1518.

Smith, J.V., Artioli, G., and Kvick, Å. (1986) Low albite, $NaAlSi_3O_8$: Neutron diffraction study of crystal structure at 13 K. American Mineralogist, 71, 727–733.

SURFER for Windows (1994) Golden Software, Inc., Golden, Colorado.

Troullier, N. and Martins, J.L. (1991) Efficient pseudopotentials for plane-wave calculations. II Operators for fast iterative diagonalization. Physical Review, B43, 8861–8869.

Wells, A.F. (1954) The geometrical basis of crystal chemistry. Part 2. Acta Crystallographica, 7, 545–554.

———(1977) Three-dimensional nets and polyedra. 268 p. Wiley, New York.

Winter, J.K., Ghose, S., and Okamura, F.P. (1977) High-temperature study of the thermal expansion and the anisotropy of the sodium atom in low albite. American Mineralogist, 62, 921–931.

Winter, J.K., Okamura, F.P., and Ghose, S. (1979) A high-temperature structural study of high albite, monalbite, and the analbite-monalbite phase transition. American Mineralogist, 64, 409–423.

Willis, B.T.M. and Pryor, A.W. (1975) Thermal vibrations in crystallography. 280 p. Cambridge University Press, London, U.K.

MANUSCRIPT RECEIVED JANUARY 22, 2002
MANUSCRIPT ACCEPTED SEPTEMBER 17, 2002
MANUSCRIPT HANDLED BY SIMON C. KOHN